Tracking Atmospheric Instabilities with the Kalman Filter. Part II: Two-Layer Results

MICHAEL GHIL* AND RICARDO TODLING†

Department of Atmospheric Sciences and Institute of Geophysics and Planetary Physics, University of California, Los Angeles, Los Angeles, California

(Manuscript received 2 January 1996, in final form 16 April 1996)

ABSTRACT

Sequential data assimilation schemes approaching true optimality for sizable atmospheric models are becoming a reality. The behavior of the Kalman filter (KF) under difficult conditions needs therefore to be understood. In this two-part paper the authors implemented a KF for a two-dimensional shallow-water model with one or two layers. The model is linearized about a basic flow that depends on latitude; this permits the one-layer (1-L) case to be barotropically unstable. Constant vertical shear in the two-layer (2-L) case induces baroclinic instability.

The stable and unstable 1-L cases were studied in Part I. In the unstable case, even a very small number of observations can keep the forecast and analysis errors from the exponential growth induced by the flow's instability. In Part II, the authors now consider the 2-L, baroclinically stable and unstable cases. Simple experiments show that both cases are quite similar to their barotropic counterparts. Once again, the KF is shown to keep the estimated flow's error bars bounded, even when a small number of observations—taken with realistic frequency—is utilized.

1. Introduction and motivation

As the amount and diversity of data available to operational meteorological centers increases, more sophisticated methods for performing data assimilation are required to optimize the use of these diverse data. There is a continuous effort by some of the major weather and climate prediction centers to base their analysis systems on more advanced assimilation methods that incorporate error-covariance dynamics. It is now widely recognized at these centers that traditional schemes like optimal interpolation (OI) or its more recent cousin, the three-dimensional variational (3D-Var) method, encounter difficulties in providing mid-range forecasts and analysis error bars that are both reliable. Due to a variety of reasons, the performance of these schemes is least reliable in the vicinity of strong atmospheric instabilities. One of these reasons is the horizontal homogeneity and vertical separability of the correlation models employed by all forecast-error covariance representations in current analysis systems (e.g., Heckley et al. 1993; Mitchell et al. 1993; Parrish and Derber 1992; Pfaendtner et al. 1995); these two assumptions break down in the presence of strong horizontal or vertical shear, respectively. The work of Bartello and Mitchell (1992) on nonseparable structure functions, and that of G. Gaspari and S. E. Cohn (1995, personal communication) on inhomogeneous correlations, presents methods for the development of more general covariance models that will eventually be used in operational forecast and analysis systems. In the process, some current analysis systems are already becoming more flexible in allowing the relatively easy implementation of general correlation representations; see, for instance, Da Silva et al.'s (1995) NASA/Goddard physical-space statistical analysis system.

The behavior of advanced data assimilation schemes in the presence of instabilities has become a topic of great interest in the past few years. Rabier and Courtier (1992) showed that a four-dimensional variational (4D-Var) method converges in following strongly unstable baroclinic developments. Two modifications of the extended Kalman filter (EKF) by Miller et al. (1994) produce very accurate and reliable state estimates in the presence of strong instabilities and nonlinearities that arise in simple dynamical systems, like the stochastically driven double-well potential and the Lorenz (1963) system. These modifications consisted in the monitoring of the innovation sequence or an appropriate estimate of the model-error statistics. Another modification of the EKF by Bürger and Cane (1994), using linearization about a previously selected flow regime, was also shown to produce reliable results when applied to the Lorenz (1963) system. As strong atmospheric and oceanic instabilities are associated with the

* Sabbatical affiliation: Laboratoire de Météorologie Dynamique du CNRS, Ecole Normale Supérieure, Paris, France.

† Current affiliation: Universities Space Research Association, NASA/Goddard Space Flight Center, Greenbelt, Maryland.

Corresponding author address: Dr. Ricardo Todling, Data Assimilation Office, Code 910.3, NASA/GSFC, Greenbelt, MD 20771.

interaction of vorticity concentrations, Ide and Ghil (1996, manuscript submitted to *Dyn. Atmos. Oceans*) have applied the EKF to vortex dynamics showing that, given a theoretically optimized observing pattern, the filter tracks the entire flow field reliably with a number of observations approximately equal to that of the isolated vortices. Ghil and Ide (1994) and Ghil (1996, manuscript submitted to *J. Meteor. Soc. Japan*) review a number of observability questions related to the EKF as applied to planetary flows, atmospheric and oceanic. The above-mentioned EKF studies were all for relatively simple models, and extension of these results to more realistic dynamics is still pending.

Todling and Ghil (1994, hereafter referred to as Part I) have described a methodology to study the behavior of the linear Kalman filter (KF) in the presence of dynamical instabilities. The linear KF represents a very idealized framework to explore the problems of atmospheric data assimilation since in actuality the presence of nonlinearities, lack of information on dynamical and statistical parameters and computational requirements make the assimilation problem much more complex. In principle, nonlinearities can be dealt with by utilizing the EKF or its modifications (Cohn 1993; Bürger and Cane 1994; Miller et al. 1994). Adaptive schemes can help estimate unknown parameters in the covariance models (Dee et al. 1985; Dee 1995) or in the deterministic part of the model dynamics (Hao 1994; Hao and Ghil 1995). The computational barrier to fully optimal EKF implementation will, most likely, always manifest itself since the tendency in numerical weather prediction has been to increase model resolution—to the extent permitted by the computing capability available at any given moment—rather than to maintain the resolution and allocate a much larger share of the increasing computational resources to more advanced data assimilation methods. Attempts like those of Boggs et al. (1995), Cohn and Todling (1996), and Verlaan and Heemink (1995; 1996, manuscript submitted to *Stochastic Hydrol. Hydraul.*) represent a few of the approaches to reduce part of the computational burden involved in performing KF-based data assimilation. A review of many of these issues is given by Ghil and Malanotte-Rizzoli (1991), Cohn (1996, manuscript submitted to *J. Meteor. Soc. Japan*), and Ghil (1996, manuscript submitted to *J. Meteor. Soc. Japan*).

The linear KF provides a very convenient framework for addressing basic and, so far, poorly understood questions like those related to unstable dynamics. Indeed, standard KF results on observability and filter convergence only exist for linear dynamics (Gelb 1974; Jazwinski 1970). The linear shallow-water model with one (1-L) or two (2-L) layers of Part I served as the testbed dynamics for addressing the desired issues. Results for the barotropically unstable 1-L case showed that the KF is able to keep the forecast and analysis errors from growing without bounds. A single well-located observation accomplishes the job of tracking the exponential growth of the instability, since the flow is dominated by the instability's known pattern and the observation basically serves to determine its amplitude. The stable 1-L version of the shallow-water model was used to study the impact of the assumed spectral characteristics of the model-error covariance matrix's spectrum on the accuracy attained by the assimilation procedure. It was found that an exponentially decaying eigenvalue spectrum allows better reduction of analysis errors. This is due to the larger correlation radii that result and, consequently, the resulting KF spreads further—and still correctly—the effect of each observation on the estimated fields; in contrast, a spectrum corresponding to energy equipartition between modes results in much smaller radii and a lessened impact of observations (see also Cohn and Parrish 1991).

In Part II of this work, we present KF assimilation experiments on the shallow-water model's 2-L version for both stable and unstable cases. Todling and Ghil (1992) presented preliminary results comparing the KF performance, discussed in Part I, with that of a simulated version of OI in the 1-L case. Todling and Cohn (1994) and Cohn and Todling (1996) carried out a careful comparison among a variety of suboptimal alternatives to the KF, including OI, for both stable and unstable barotropic dynamics. A similar comparative study for the present 2-L, baroclinic case is not expected to yield results that differ significantly from the 1-L case.

The purpose of Part II is, therewith, to study further the performance of sequential estimation methods in the presence of strong baroclinic instability. In section 2 we briefly recall the methodology of Part I and the atmospheric model under consideration here. Section 3 presents results for the 2-L assimilation experiments with stable and unstable dynamics. Conclusions are drawn in section 4.

2. Model and assimilation scheme

The model used in this work, as described in Part I, is governed by the 1-L or 2-L shallow-water equations linearized about a basic state with no meridional velocity component and a zonal wind that can depend on latitude. In Part I, we have used the 1-L barotropic version of the model simulating both stable and unstable situations, depending on the choice of the basic zonal-wind profile. We have constructed, for the stable and unstable cases of both the 1- and 2-L model versions, an error covariance matrix based on the slow modes of each system. These covariance matrices were used in the data assimilation experiments as model error covariances and initial analysis error covariances, following Cohn and Parrish (1991). In particular, we have looked at different model error spectra and concluded that strong energy decay with the modes' wavenumber is fundamental in specifying model errors and induces significant forecast and analysis error reduction in the assimilation process.

TABLE 1. The 2-L shallow-water model parameters.

	Stable	Unstable
Number of grid points $I = J - 1$	16	16
Extent of channel $L_x = L_y$	6000 km	4000 km
Grid size $\Delta x = \Delta y$	385 km	250 km
Time step Δt	10 min	5 min
Coriolis parameter f_0	1.0×10^{-4} s^{-1}	1.0×10^{-4} s^{-1}
β-plane parameter β	1.5×10^{-11} m^{-1} s^{-1}	1.5×10^{-11} m^{-1} s^{-1}
Upper-layer mean geopotential height Φ_1	1.5×10^{4} m^2 s^{-2}	10×10^{4} m^2 s^{-2}
Lower-layer mean geopotential height Φ_2	1.5×10^{4} m^2 s^{-2}	3×10^{4} m^2 s^{-2}
Upper-layer mean velocity U_1	20 m s^{-1}	20 m s^{-1}
Lower-layer mean velocity U_2	20 m s^{-1}	10 m s^{-1}
Density ratio between the two layers α_2	0.95	0.95

Due to the linearity of the problem, it suffices to concentrate on the behavior of the error covariances (Ghil et al. 1981). Hence, we refer only to the covariance evolution equation,

$$\mathbf{P}_k^f = \mathbf{\Psi}_k \mathbf{P}_{k-1}^a \mathbf{\Psi}_k^{\mathrm{T}} + \mathbf{Q}_k, \tag{2.1}$$

and covariance update equation,

$$\mathbf{P}_k^a = (\mathbf{I} - \mathbf{K}_k \mathbf{H}_k)\mathbf{P}_k^f, \tag{2.2}$$

where optimality is achieved by using the Kalman gain matrix $\mathbf{K}_k$,

$$\mathbf{K}_k = \mathbf{P}_k^f \mathbf{H}_k^{\mathrm{T}} (\mathbf{H}_k \mathbf{P}_k^f \mathbf{H}_k^{\mathrm{T}} + \mathbf{R}_k)^{-1}, \tag{2.3}$$

at every time t_k. For the sake of consistency with Part I, we continue to adopt here the notation of Ghil (1989) and Ghil and Malanotte-Rizzoli (1991), rather than the "World Meteorological Organization standard" proposed by Ide et al. (1996, manuscript submitted to *J. Meteor. Soc. Japan*). A detailed explanation of the quantities in the equations above can be found for instance in Ghil (1989). Briefly, $\mathbf{P}_k^{f,a}$ refers to the forecast (f) and analysis (a) error covariance matrices; $\mathbf{Q}_k$ and $\mathbf{R}_k$ are the error covariances for the model and observations, respectively; and $\mathbf{H}_k$ is the interpolation operator that takes the forecast quantities to observation locations.

The matrix $\mathbf{\Psi}_k$ represents the model dynamics; in the present context, it is the operator corresponding to the finite-difference discretization of the linear 2-L shallow-water model:

$$\frac{\partial u_n}{\partial t} + U_n \frac{\partial u_n}{\partial x} + \frac{\partial}{\partial x}(\alpha_n \phi_1 + \phi_2) - (f - U_n')v_n = 0, \tag{2.4a}$$

$$\frac{\partial v_n}{\partial t} + U_n \frac{\partial v_n}{\partial x} + \frac{\partial}{\partial y}(\alpha_n \phi_1 + \phi_2) + f u_n = 0, \tag{2.4b}$$

$$\frac{\partial \phi_n}{\partial t} + U_n \frac{\partial \phi_n}{\partial x} + \Phi_n\left(\frac{\partial u_n}{\partial x} + \frac{\partial v_n}{\partial y}\right) + \Phi_n' v_n = 0, \tag{2.4c}$$

where u_n, v_n are the velocity perturbations, ϕ_n are geopotential perturbations, $f = f_0 + \beta y$ is the Coriolis parameter, and the basic flow satisfies

$$f U_n + (\alpha_n \Phi_1 + \Phi_2)' = 0. \tag{2.5}$$

The primes denote differentiation of variables depending on y only, $n = 1, 2$ refers to the upper and lower layers, respectively, and $\alpha_1 = 1$, $\alpha_2 = \rho_1/\rho_2$, where ρ_n are the densities of each layer.

3. Results

a. Stable case

In this section we apply the KF to the stable case of the 2-L shallow-water model described in Part I, using the model parameters given in Table 1; this table is identical to Table 3 of Part I and is reproduced here for the reader's convenience. The difference between this system and the barotropic 1-L system studied in Part I is that the fluid densities in the two layers are different and their ratio is given by the parameter α_2. In our data assimilation experiments for the stable case we assume that the two model layers are of equal thickness—equal to one-half of the total height of the 1-L atmosphere discussed in greater detail in Part I (see Table 1 there)—and represent the 500- and 850-mb levels of the atmosphere, respectively. Assuming the observations to be composed of radiosondes measuring wind and heights at 6-h intervals, their standard deviations follow Dey and Morone (1985) and are equal to

$$\sigma_{h_1}^o = 12.1 \text{ m}, \quad \sigma_{u_1}^o = 3.4 \text{ m s}^{-1}, \quad \sigma_{v_1}^o = 3.4 \text{ m s}^{-1}, \tag{3.1}$$

$$\sigma_{h_2}^o = 8.0 \text{ m}, \quad \sigma_{u_2}^o = 1.8 \text{ m s}^{-1}, \quad \sigma_{v_2}^o = 1.8 \text{ m s}^{-1}. \tag{3.2}$$

We consider a network with 80 stations scattered randomly over the channel, as depicted in Fig. 1 for the model domain using 16×17 grid points.

We start the assimilation experiments by taking an initial analysis error covariance matrix 200 times larger than the model error covariance matrix, which was con-

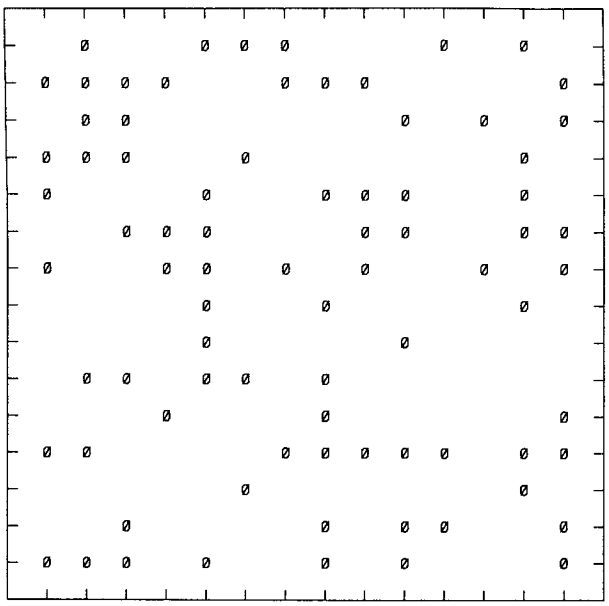

FIG. 1. Observational network composed of 80 stations positioned randomly at gridpoint locations.

structed following the procedure described in Part I, with an exponentially decaying energy spectrum. This choice of spectrum is made on the basis of the studies in Part I, where it was shown that such a spectrum allows the assimilation scheme to achieve smaller analysis errors. In Fig. 2 we show the results for experiment S1 in Table 2. The evolution in time of the domain-averaged expected root-mean-square (ERMS) error, up to 2 days, is used as an indicator of the behavior of the KF. The errors in each model variable are displayed separately.

Three main results emerge from this picture. First, the ERMSs asymptote toward a bounded, periodic behavior, with a period of 6 h and the minima occurring at update time. This behavior was noticed already in the one-dimensional (1D), linear, shallow-water model of Ghil et al. (1981) and Cohn (1982) and many KF studies since. It was exploited in a computationally efficient KF implementation of Fukumori et al. (1993); see also Ghil (1996, manuscript submitted to *J. Meteor. Soc. Japan*) for additional references on computational implications of this periodicity. Second, the errors evolve quite similarly in the two layers, with anal-

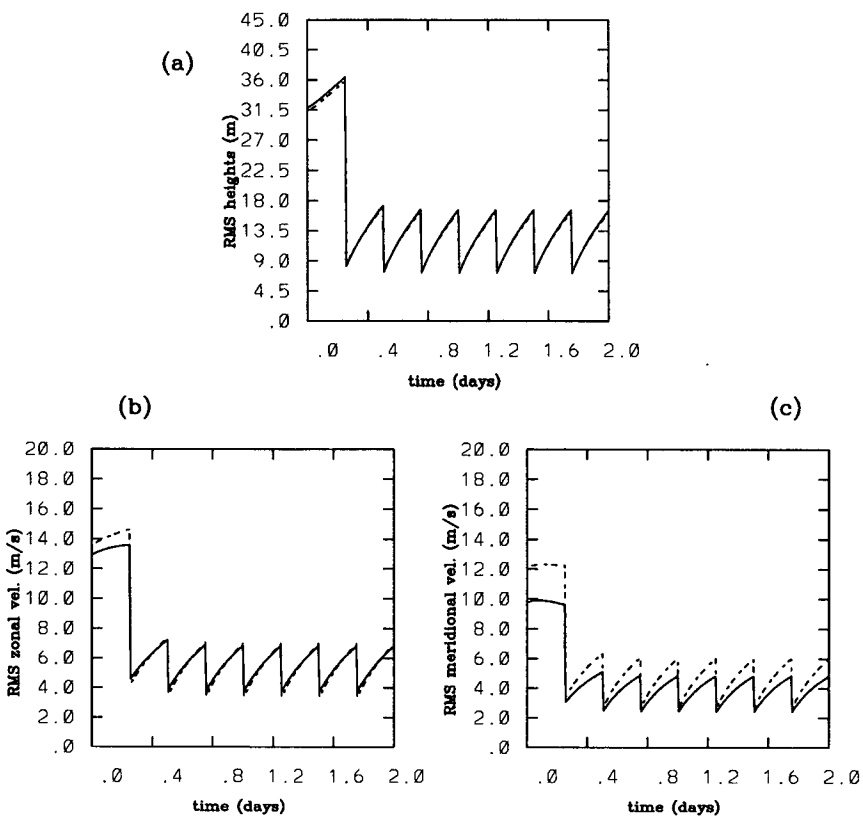

FIG. 2. Domain-averaged ERMS errors for stable case; the assimilation uses 80 radiosondes observing all variables in both layers at 6-h intervals for 2 days. Panels (a), (b), and (c) are for heights, zonal, and meridional winds, respectively. Dashed lines are for lower-layer quantities and solid lines for upper-layer quantities; velocity errors in meters per second and height errors in meters.

TABLE 2. Experiments performed with the 2-L shallow-water model.

Experiment number	Observation pattern	Observation frequency (h)
Stable case		
S1	80 points/both layers	6
S2	80 points/lower layer only	6
Unstable Case		
U1	No update	0
U2	Point (8, 9)	6
U3	Point (8, 14)	6
U4	Line $(8, j)$, $j = 2, \ldots, 16$	6
U5	80 points	6

ysis errors approximately the same for each pair of corresponding variables. Third, the analysis errors in the meridional wind and the heights at both levels are just about equal to the corresponding smallest observational error level, that is, the lower-layer observational errors; the zonal wind errors are somewhat above that level, a fact that is also true for the 1-L stable barotropic case (see Fig. 4 of Cohn and Parrish 1991). The upper-layer height and meridional wind reach error levels that are in fact below the observational error level in this layer. It follows that information propagates in this stable case rather efficiently in the vertical—from the lower, more accurately observed level to the upper, less well observed one—as in the horizontal, from observed to unobserved grid points. Experiments with an increasing number of observations (not shown) confirm that the errors eventually drop well below the observational error level in both layers and all three fields.

The relative inefficiency of error reduction in the zonal wind—noticed already in the 1D, 1-L shallow-water model of Ghil et al. (1981) and in the 2D, 1-L model of Cohn and Parrish (1991) and of Part I—is probably associated with the fact that the errors in observing this component and the meridional one are equal, while the actual magnitudes are not. In a Rossby wave—the dominant phenomenon in a stable atmosphere, whether 1- or 2-L—the major quasi-geostrophic balance occurs between zonal perturbations in the height gradient and meridional ones in the wind (e.g., Fig. 2.7 in Ghil and Childress 1987). As a result, dynamic perturbations in the zonal wind are

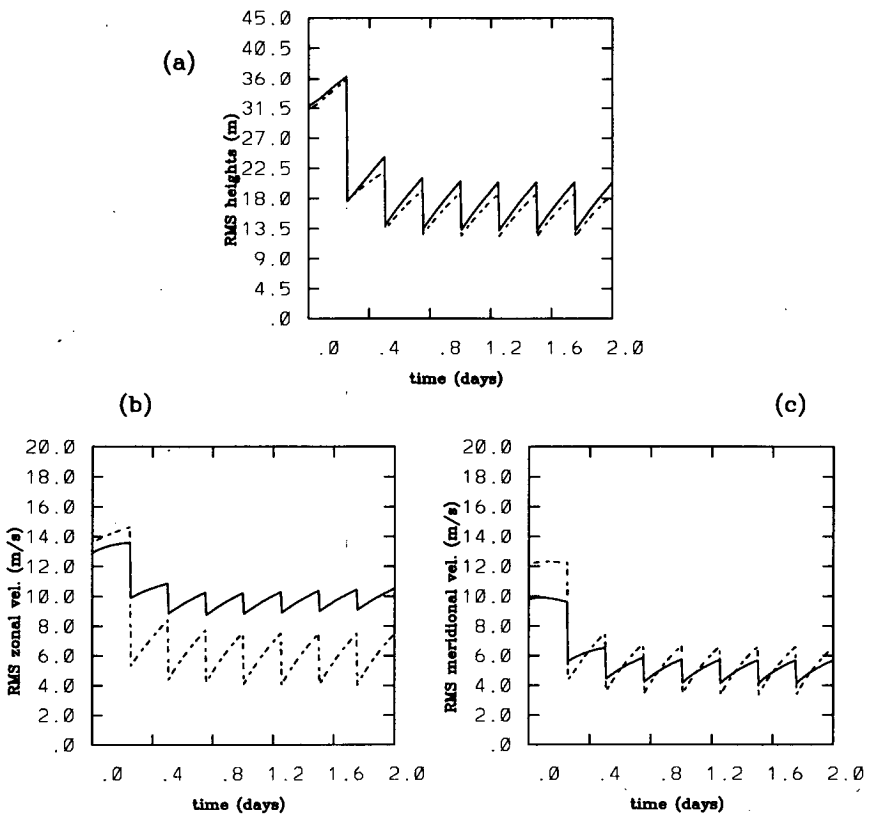

FIG. 3. Same as in Fig. 2 but with an observational network composed of 80 radiosondes observing in the lower layer only, at 6-h intervals.

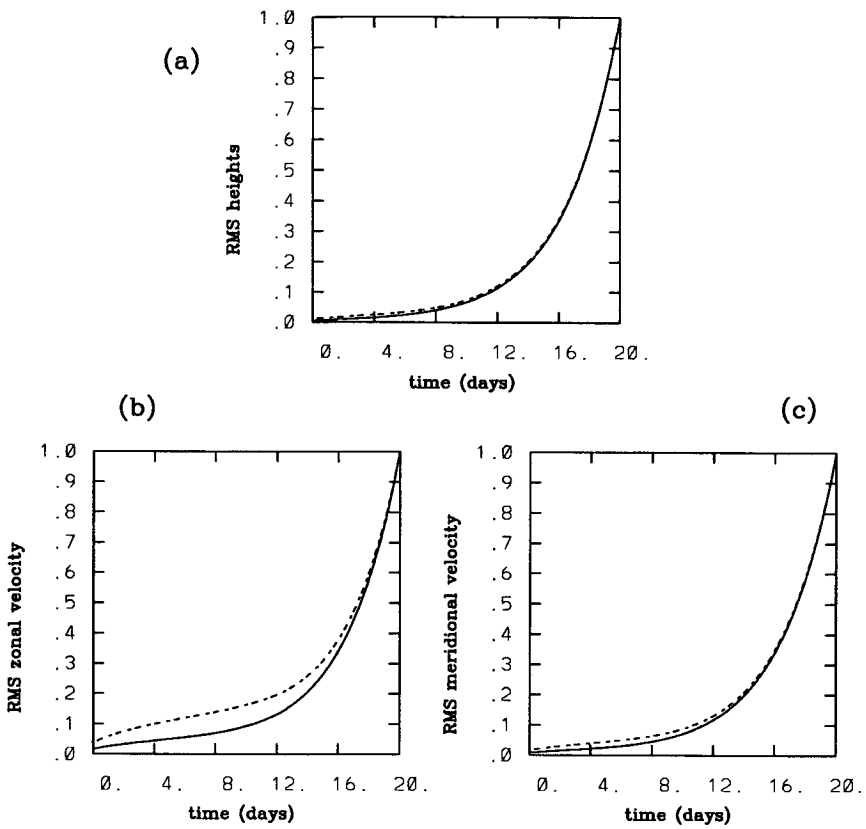

FIG. 4. Same as in Fig. 2 but for the unstable case with no update. Curves are now normalized by their corresponding maximum values and extend to day 20.

typically quite a bit smaller than in the meridional winds, while the measurement errors in the two wind components are equal for all observing systems in practical use.

As in the 1-L case, the forecast error correlations (not shown) resemble very closely the model error correlations shown in Fig. 7 of Part I. This has been discussed in detail by Cohn and Parrish (1991) and also in Part I for the barotropic 1-L case; in short, it is due to the fact that the observing network is quite uniform, as depicted in Fig. 1. Figure 7 of Part I shows wind–wind correlations that are extremely localized, especially those related to cross correlations that involve a zonal wind component in either layer (compare also Fig. 3 of Part I for the stable 1-L case).

The stable case is illustrated further in experiment S2 of Table 2, with results displayed in Fig. 3. Now the 80 radiosondes of Fig. 1 only observe in the lower layer. The same update interval of 6 h is used, as indicated in Table 2, and the experiment is followed for 2 days as before. Wind and mass error reduction occur in the upper layer, too, due to the interaction between layers. The number of observations in the lower layer does not suffice, however, to lower the analysis errors below the observational error levels there. Both wind error components in the lower layer are only slightly less accurate than in experiment S1 (Fig. 2). The height error in the bottom layer increases significantly, though, due to not observing the heights in the layer above: the height–height forecast error cross correlations between the two layers are strong, while the wind–wind ones are not (see again Fig. 7 of Part I). The largest increase in error level occurs in the upper-layer zonal wind for the reasons already stated.

b. Unstable case

To simulate the unstable case, the model parameters are changed according to the specifications in Table 1. The layer thicknesses are increased to prevent the interface between them from intersecting the free surface or the surface of the earth (see Todling and Ghil 1990). The first experiment we conduct, U1 in Table 2, includes no error covariance update due to observations, that is, the initial analysis error covariance evolves solely according to the dynamics $\mathbf{\Psi}_k$ as we make, in addition, the perfect model assumption of $\mathbf{Q}_k = \mathbf{0}$ at all times. Hence the error covariance evolution in (2.1) reduces to that of the predictability error covariance $\mathbf{P}_k^p$:

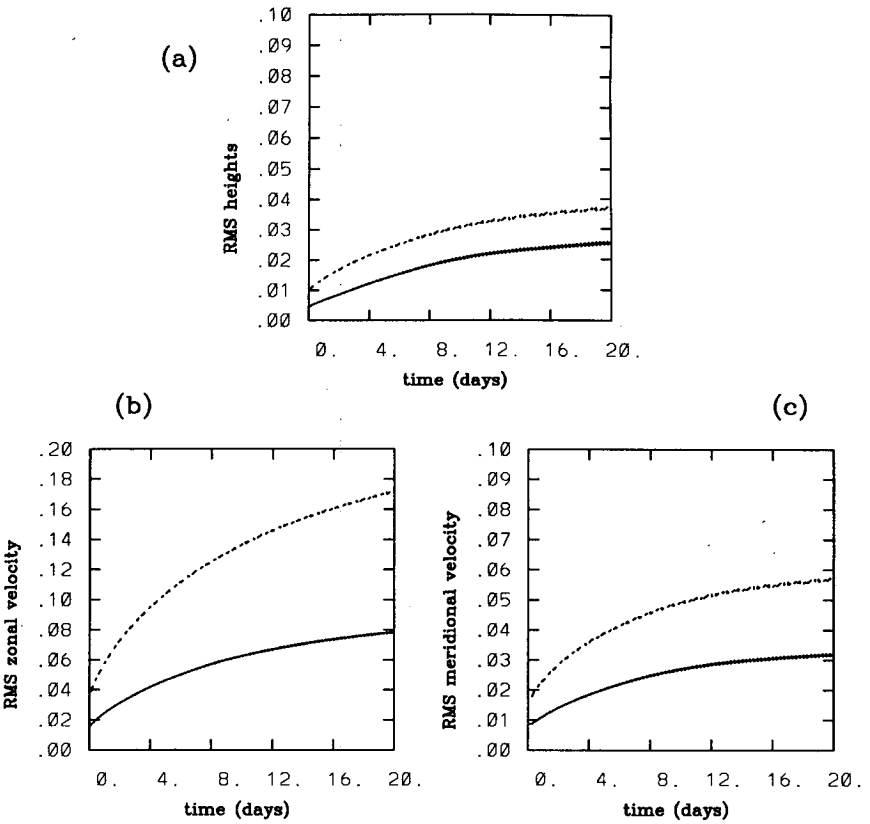

FIG. 5. As in Fig. 4 but with update every 6 h of all six variables of the model at the central grid point (8, 9). Errors normalized by their corresponding maximum values for the case with no update (see Fig. 4).

$$\mathbf{P}_k^p = \mathbf{\Psi}_k \mathbf{P}_{k-1}^a \mathbf{\Psi}_k^{\mathrm{T}}. \tag{3.3}$$

Equation (3.3) allows us to study the effect of the baroclinic instability on $\mathbf{P}_k^f = \mathbf{P}_k^p$ without interference from either observations or model errors. As for the 1-L unstable case (see Fig. 13a of Part I), Fig. 4 shows the ERMS error averaged over the whole domain, for all variables of the model up to day 20. Each curve has been normalized by its maximum value. Errors grow exponentially as the instability develops.

Following the experiments reported in Part I for the unstable barotropic case, we adopt again the setup of a single-station observation, while keeping—unlike in Part I—the perfect-model assumption of the no-observation experiment U1. We assume for the present, unstable case that the two model layers simulate the 250- and the 500-mb levels of the atmosphere, respectively, and we take observation errors to be

$$\sigma_{h_1}^o = 25.4 \text{ m}, \quad \sigma_{u_1}^o = 5.9 \text{ m s}^{-1}, \quad \sigma_{v_1}^o = 5.9 \text{ m s}^{-1}, \tag{3.4}$$

$$\sigma_{h_2}^o = 12.1 \text{ m}, \quad \sigma_{u_2}^o = 3.4 \text{ m s}^{-1}, \quad \sigma_{v_2}^o = 3.4 \text{ m s}^{-1}, \tag{3.5}$$

according to the values used for these levels at the National Meteorological Center (NMC) and listed in Dey and Morone (1985). The observational errors are, therewith, larger in this unstable case, with the errors in the lower layer now equal to those used for the upper layer in the earlier, stable case.

Experiments U2 and U3 have all six model variables being observed at 6-h intervals. In experiment U2 the observation is located along the symmetry axis of the channel, at grid point (8, 9), while in experiment U3 the observing station is moved northward to point (8, 14). Figures 5 and 6 display the ERMS error evolution for the 20-day assimilation period. Each of the curves in the figure has been normalized by its corresponding maximum value in experiment U1, the control run.

The errors are now kept bounded due to the frequent update and the KF's knowledge of the model dynamics, and hence of the instability's spatial pattern. In contrast to the unstable 1-L case (see Figs. 13b and 14a,b of Part I), in the 2-L case there is very little difference between observing in the middle of the channel, as in experiment U2, or at another location, as in experiment U3. This is a consequence of the absence of the meridionally dependent jet that was present in the unstable

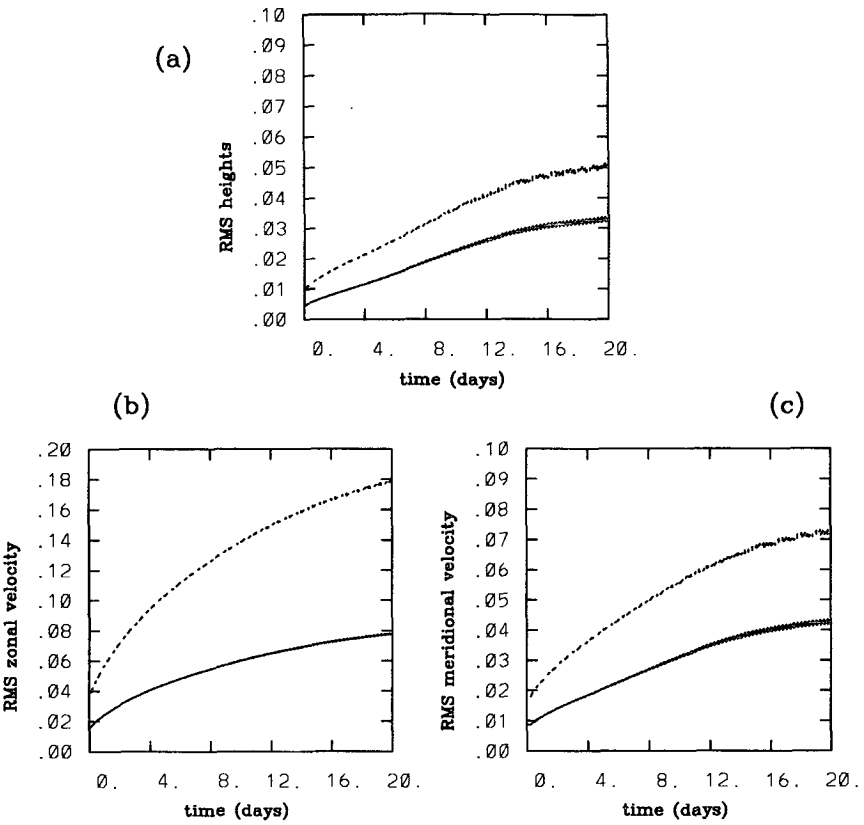

FIG. 6. As in Fig. 5 but with observation point moved northward to grid point (8, 14).

case studied in Part I for the 1-L model. The relatively small difference that is present between corresponding panels in Figs. 5 and 6 can be attributed to the β effect. While the zonal wind errors are again the largest relative to the no-update case (notice change in vertical scale), there is almost no change with the position of the observation station.

The forecast and analysis errors of experiments U2 and U3 do not grow exponentially anymore. Still, a single observing station is not sufficient to actually reduce the initial errors in those cases. In experiment U4, we observe along a meridional section $(8, j)$, $j = 2, \cdots, 16$, in the upper layer only. Figure 7 shows that, in this case, the initial errors are reduced gradually and steadily, and there is no growth due to flow instabilities at all. The errors in the lower layer are somewhat higher than the errors in the upper layer since the observations are taken only in the latter. It is interesting to notice that observing along a meridional section solely in one layer is enough to track the instability. In fact, asymptotic error levels using only 45 scalar observations in this unstable case—but without model errors—are substantially lower than in the stable case where model errors are present and 480 scalars are being observed (see Fig. 2).

Further aspects of experiment U4 are shown in Fig. 8 by plotting maps of the forecast-error standard deviation in the height fields for both layers. Figure 8a displays the height error fields at day 2, while Fig. 8b is for day 5. The contour interval of 1 m is the same in the two panels, showing immediately the decrease in the overall error field from day 2 to day 5, as already seen in the ERMS plots in Fig. 7.

Figure 8 illustrates the interaction between the two layers, with the errors in the upper layer, where measurements are taken, being only slightly smaller than in the lower layer. It is in fact remarkable that the strong gradient in the error fields, which is indubitably due to the observation pattern, is much clearer in the lower layer, where no observation is actually taken. This is a consequence of the fact that the KF utilizes the dynamics optimally during the assimilation procedure and that the northwest–southeast propagation of Rossby waves (Held 1983) has larger amplitude in the upper layer. The overall propagation of information from the northwest to the southeast has already been observed in the studies of Parrish and Cohn (1985) and Todling (1992), for the 1-L, barotropically stable version of this model. The novel and interesting fact apparent here is that this propagation is more pronounced in the upper

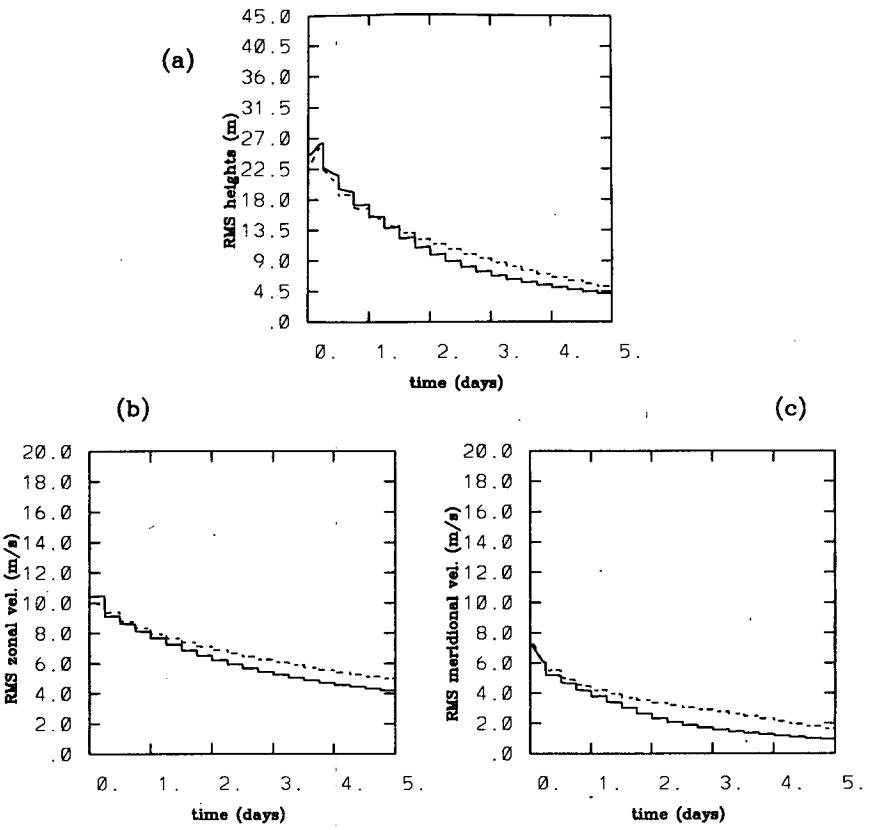

FIG. 7. As in Fig. 5 but observations are located along the line $(8, j), j = 2, \cdots, 16$, in the upper layer only. Curves are not normalized and shown out to 5 days only.

layer, where the observations are taken, while the signature of the observing network lasts longer in the unobserved lower layer.

The maps of forecast-error standard deviations in the zonal wind are shown in Fig. 9. They still demonstrate considerable persistence of the observing pattern in the reduced errors of both layers. The propagation of information in the zonal wind is along the zonal direction in both layers, with relatively large error gradients left along the north and south walls, as shown already in the barotropic stable version of Parrish and Cohn (1985) and Todling (1992).

For the final experiment, we consider nonzero model errors, constructed exclusively on the basis of the slow modes of the unstable dynamics, as explained in sections 3b–d of Part I. We use a decaying spectrum for the model-error covariance matrix as before (see section 3a above). Experiment U5 of Table 2 uses the observational network of Fig. 1 with radiosondes in both layers. The assimilation results are shown in Fig. 10.

The error evolution is practically indistinguishable from that in Fig. 2: the error growth in between observations is completely dominated by the model error, with no visible contribution from the exponential growth due to the model dynamics. Interestingly enough, the only analysis errors not reaching levels below the observation threshold are the ones for the zonal component of the velocity in the lower layer. Comparing this result with the one shown in Fig. 2—where the observation errors are much lower—for the stable no-shear case, we are led to conclude that the presence of shear and the instability it entails enhance the exchange of information between the layers and the associated analysis-error reduction.

4. Concluding remarks

In Part I of this work (Todling and Ghil 1994) we have set up one- and two-layer (1-L and 2-L) versions of a 2D, linear, shallow-water model in a midlatitude β channel, with periodicity in the zonal direction. The performance of the KF in assimilating sparse and inaccurate data was studied there for the 1-L version, both for a stable and an unstable basic flow profile, as a function of data distribution and the assumptions made in constructing the model-error covariance matrix. The main conclusions of Part I were that the latter assumptions matter and that the error variance (or energy) should decay with wavenumber; that the KF is able to keep forecast and analysis errors bounded in the

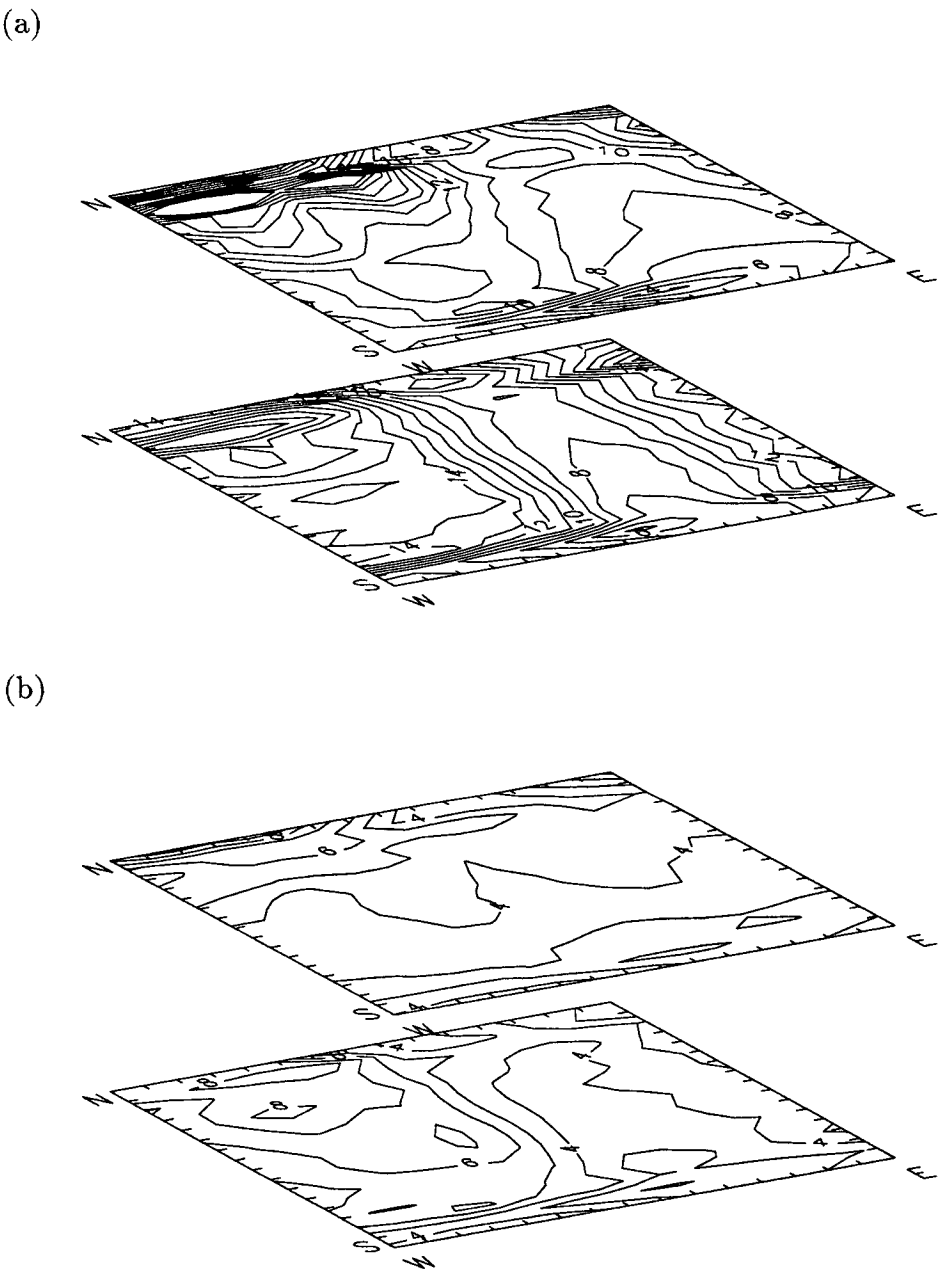

FIG. 8. Forecast error standard deviation in the height field in both layers, for observations along a meridional section (same as Fig. 7): (a) at day 2 and (b) at day 5. Contour interval is 1 m.

presence of strong barotropic instability, while using very few observations; and that forecast-error correlations become quite anisotropic and inhomogeneous due to the instability.

In the present paper, Part II of the work, we have studied KF performance for the model's 2-L version in a stable and an unstable case. Baroclinic instability was induced by vertical shear between the two layers with no horizontal shear present. The key point of the results, as in Part I, is that the KF's knowledge of the dynamics—and hence of the instability's spatial pattern—helps track the unstable flow, even when using observations that are quite sparse and inaccurate.

To simulate the irregular network of conventional observing stations over a relatively data-dense area like the Northern Hemisphere's land areas, we have used a random pattern (Fig. 1) with 80 stations out of a total of $16 \times 17 = 272$ (horizontal) grid points; that is, less

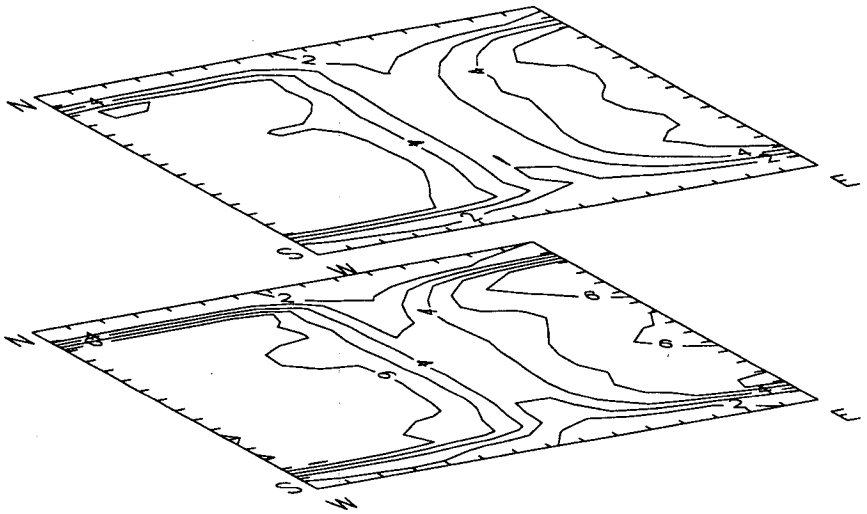

FIG. 9. As in Fig. 8 but for the errors in the zonal wind. Only the result at day 5 is displayed, and the contour interval is 1 m s^{-1}.

than 30% of the points, at most, are observed. In the stable case, observing all model variables, h, u, and v, in both layers (that is, six scalars per horizontal grid point) suffices, when starting with very high initial errors, to reduce the ERMS errors in all variables to the observational error levels, taken equal to those used at

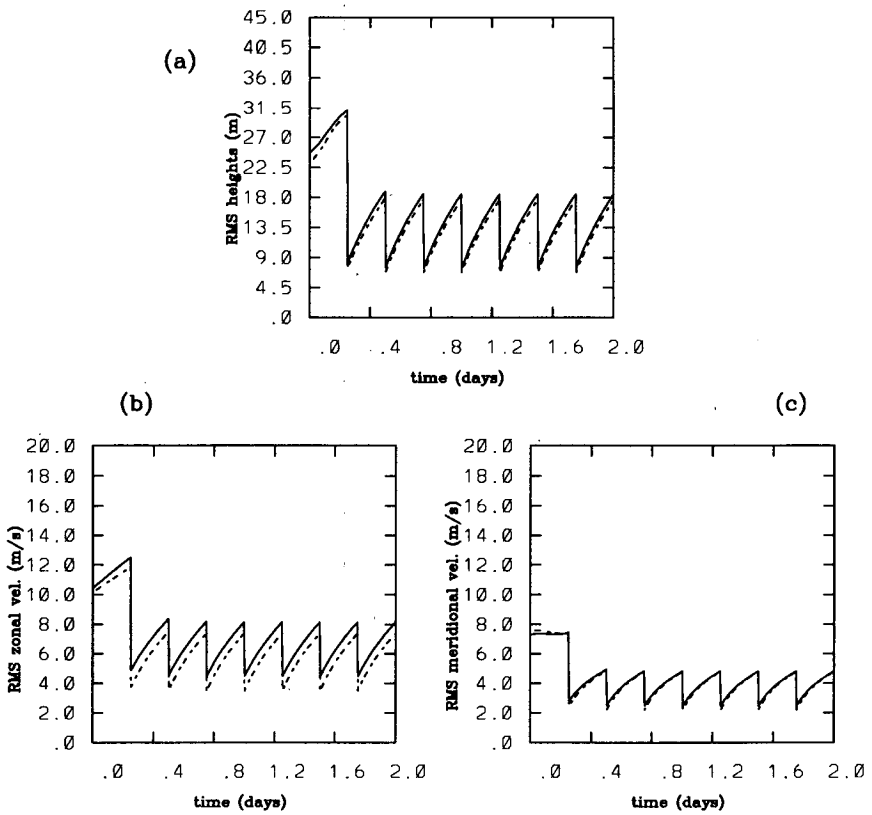

FIG. 10. As in Fig. 5 but with the 80 observing stations of Fig. 1, used in both layers. The perfect model assumption is not made in this case, and curves are not normalized.

NMC for the corresponding pressure levels (Fig. 2), over a 2-day interval.

The only exception are the zonal winds, a fact already observed by Ghil et al. (1981) and Cohn and Parrish (1991) in simpler, 1-L versions of this model (first 1D and then 2D), which can be explained by the large observational errors in this component, relative to its total magnitude. Using lower-layer observations only at the same stations still leads to an asymptotically periodic ERMS evolution (Fig. 3), with only the upper-layer zonal wind showing a substantial, but not disastruous, loss of accuracy. In this case we deal with a mere 13% of scalar model variables being observed every 6 h for a few update times, and the relative accuracy of the results is well explained by the in-layer and layer-to-layer spatial (cross-) correlations of the various fields, as shown in Todling (1992) and Part I.

In the absence of either observations or model noise, the ERMS in the unstable case grows exponentially, after day 5. The initial transient apparent in Fig. 4 is due to lack of self-adjointness of the linear operator defined by Eqs. (2.4) and (2.5). This leads to faster growth of certain modes of the short-term symmetric propagator, overtaken eventually by the fastest modal instability of the linear operator itself [see Lacarra and Talagrand (1988) and the discussion of Fig. 4 of Part I]. Maintaining, for illustration purposes, the hypothesis of no model errors (implicit in the adjoint-method implementations of 4D-Var), we have shown that a single station, observing in both layers, suffices to keep the ERMS bounded (Fig. 5). Since the basic state in the baroclinically unstable case studied here has only vertical shear, the position of this single station matters relatively little (compare Fig. 6 to Fig. 5), unlike in the barotropically unstable case of Part I, where horizontal shear is present and of paramount importance.

In the absence of model errors, observations along a meridional cross section, in the upper layer only, suffice to reduce the error in all variables, in both layers, asymptotically to zero (Fig. 7). Thus, "knowing" the spatial pattern of the instability, it suffices for the KF to observe the unstable wave as it travels through, as was already the case for the neutrally stable waves in the 1D, 1-L model of Ghil et al. (1981, see Fig. 2 there): for m update times, the error is reduced in proportion to $m^{-1/2}$. The analogy with the well-known case of repeated independent observations of a single scalar, constant in time, is striking and illustrates the full ingenuity of the KF.

Finally, reinstating the model noise to the same level and with the same decaying spectrum as in the stable case (Fig. 2), but restricted to the slow modes only [following Phillips (1986) and Cohn and Parrish (1991) in the 1-L case], still permits one to attain an asymptotically periodic ERMS evolution in less than 2 days (Fig. 10) when using the random observing pattern of Fig. 1. In fact, the analysis and forecast error levels are lower relative to the observational error levels than for the stable case of Fig. 2, showing the dominant role of the instability in propagating flow information.

It is clear that nonlinear saturation and interaction of multiple instabilities, barotropic and baroclinic, in a more realistic model will complicate substantially the optimistic picture obtained in this two-part study. But the study's results do encourage us to hope that computationally efficient implementations of the extended Kalman filter will permit the accurate tracking of these interacting instabilities with the limited number of very diverse observations actually available for most atmospheric and oceanic problems.

Acknowledgments. This research was supported by a scholarship program from Brazil's CNPq (RT), NASA Grant NAG-5713 and ONR Grant N0014-89-J-1845 (MG and RT), and—in its final stages—by the Condorcet Visiting Chair of the Ecole Normale Supérieure, Paris (MG), and NASA's Data Assimilation Office at the Goddard Space Flight Center (RT). The numerical results were obtained through the helpful cooperation of the NASA Center for Computational Sciences at the Goddard Space Flight Center on its Cray C90. Comments from David Parrish and an anonymous reviewer helped improve the presentation. This is contribution number 4624 from UCLA's Institute of Geophysics and Planetary Physics.

REFERENCES

Bartello, P., and H. L. Mitchell, 1992: A continuous three-dimensional model of short-range forecast error covariances. *Tellus,* **44A,** 217–235.

Boggs, D., M. Ghil, and C. Keppenne, 1995: A stabilized sparse-matrix U–D square-root implementation of a large-state extended Kalman filter. *Proc. Int. Symp. on Assimilation of Observations in Meteorology and Oceanography,* Tokyo, Japan, World Meteor. Org., 219–224.

Bürger, G., and M. A. Cane, 1994: Interactive Kalman filtering. *J. Geophys. Res.,* **99,** 8015–8031.

Cohn, S. E., 1982: Methods of sequential estimation for determining initial data in numerical weather prediction. Ph.D. thesis, Courant Institute of Mathematical Sciences, New York University, 183 pp.

——, 1993: Dynamics of short-term univariate forecast error covariances. *Mon. Wea. Rev.,* **121,** 3123–3149.

——, and D. F. Parrish, 1991: The behavior of forecast error covariances for a Kalman filter in two dimensions. *Mon. Wea. Rev.,* **119,** 1757–1785.

——, and R. Todling, 1996: Approximate data assimilation schemes for stable and unstable dynamics. *J. Meteor. Soc. Japan,* **74,** 63–75.

Da Silva, A., J. Pfaendtner, J. Guo, M. Sienkiewicz, and S. E. Cohn, 1995: Assessing the effects of data selection with DAO's physical-space statistical analysis system. *Proc. Int. Symp. on Assimilation of Observations in Meteorology and Oceanography,* Tokyo, Japan, World Meteor. Org., 273–278.

Dee, D. P., 1995: On-line estimation of error covariance parameters for atmospheric data assimilation. *Mon. Wea. Rev.,* **123,** 1128–1145.

——, S. E. Cohn, A. Dalcher, and M. Ghil, 1985: An efficient algorithm for estimating noise covariances in distributed systems. *IEEE Trans. Autom. Control,* **AC-30,** 1057–1065.

Dey, C. H., and L. L. Morone, 1985: Evolution of the National Meteorological Center global data assimilation system: January 1982–December 1983. *Mon. Wea. Rev.*, **113,** 304–318.

Fukumori, I., J. Benveniste, C. Wunsch, and D. B. Haidvogel, 1993: Assimilation of sea surface topography into an ocean circulation model using a steady-state smoother. *J. Phys. Oceanogr.*, **23,** 1831–1855.

Gelb, A., 1974: *Applied Optimal Estimation.* MIT Press, 374 pp.

Ghil, M., 1989: Meteorological data assimilation for oceanographers. Part I: Description and theoretical framework. *Dyn. Atmos. Oceans,* **13,** 171–218.

——, and S. Childress, 1987: *Topics in Geophysical Fluid Dynamics: Atmospheric Dynamics, Dynamo Theory and Climate Dynamics.* Springer-Verlag, 485 pp.

——, and P. Malanotte-Rizzoli, 1991: Data assimilation in meteorology and oceanography. *Advances in Geophysics,* Vol. 33, Academic Press, 141–266.

——, and K. Ide, 1994: Extended Kalman filtering for nonlinear vortex systems: An example of observing-system design. *Data Assimilation for Modelling the Ocean in a Global Change Perspective,* P. P. Brasseur and J. C. J. Nihoul, Eds., Springer-Verlag, 167–193.

——, S. Cohn, J. Tavantzis, K. Bube, and E. Isaacson, 1981: Applications of estimation theory to numerical weather prediction. *Dynamic Meteorology: Data Assimilation Methods,* L. Bengtsson, M. Ghil, and E. Källén, Eds., Springer-Verlag, 139–224.

Hao, Z., 1994: Data assimilation for interannual climate-change prediction. Ph.D. thesis, University of California, Los Angeles, 224 pp.

——, and M. Ghil, 1995: Sequential parameter estimation for a coupled ocean-atmosphere model. *Proc. Int. Symp. on Assimilation of Observations in Meteorology and Oceanography,* Tokyo, Japan, World Meteor. Org., 181–186.

Heckley, W. A., P. Courtier, J. Pailleux, and E. Andersson, 1993: The ECMWF variational analysis: General formulation and use of background information. *Proc. ECMWF Workshop on Variational Assimilation,* Reading, United Kingdom, ECMWF, 49–94.

Held, I. M., 1983: Stationary and quasi-stationary eddies in the extratropical troposphere: Theory. *Large-Scale Dynamical Processes in the Atmosphere,* B. Hoskins and R. Pearce, Eds., Academic Press, 127–168.

Jazwinski, A. H., 1970: *Stochastic Processes and Filtering Theory.* Academic Press, 376 pp.

Lacarra, J. F., and O. Talagrand, 1988: Short-range evolution of small perturbations in a barotropic model. *Tellus,* **40A,** 81–95.

Lorenz, E. N., 1963: Deterministic nonperiodic flow. *J. Atmos. Sci.,* **20,** 130–141.

Miller, R. N., M. Ghil, and F. Gauthiez, 1994: Advanced data assimilation in strongly nonlinear dynamical systems. *J. Atmos. Sci.,* **51,** 1037–1056.

Mitchell, H. L., C. Charette, S. J. Lambert, J. Hallé, and C. Chouinard, 1993: The Canadian global data assimilation system: Description and evaluation. *Mon. Wea. Rev.,* **121,** 1467–1492.

Parrish, D. F., and J. C. Derber, 1992: The National Meteorological Center's spectral statistical-interpolation analysis system. *Mon. Wea. Rev.,* **120,** 1747–1763.

——, and S. E. Cohn, 1985: A Kalman filter for a two-dimensional shallow-water model: Formulation and preliminary experiments. Office Note 304, 64 pp. [Available from National Meteorological Center, 5200 Auth Rd., Camp Springs, MD 20746.]

Pfaendtner, J., S. Bloom, D. Lamich, M. Seablom, M. Sienkiewicz, J. Stobie, and A. da Silva, 1995: Documentation of the Goddard Earth Observing System (GEOS) data assimilation system—Version 1. NASA Tech. Memo. 104606, Vol. 4. [Available online from http://dao/gsf.nasa.gov/subpages/tech-reports.html.]

Phillips, N. A., 1986: The spatial statistics of random geostrophic modes and first-guess errors. *Tellus,* **38A,** 314–332.

Rabier, F., and P. Courtier, 1992: Four-dimensional assimilation in the presence of baroclinic instability. *Quart. J. Roy. Meteor. Soc.,* **118,** 649–672.

Todling, R., 1992: The Kalman filter for two-dimensional stable and unstable atmospheres. Ph.D. thesis, University of California, Los Angeles, 171 pp.

——, and M. Ghil, 1990: Kalman filtering for a two-layer, two-dimensional shallow-water model. *Proc. Int. Symp. Assimilation of Observations in Meteorology and Oceanography,* Clermont-Ferrand, France, World Meteor. Org., 454–459.

——, and ——, 1992: Comparisons between the Kalman filter and optimal interpolation for two-dimensional atmospheres. *Proc. Seventh Brazilian Meteorology Congress,* São Paulo, Brazil, Brazilian Meteor. Org., 660–664.

——, and ——, 1994: Tracking atmospheric instabilities with the Kalman filter. Part I: Methodology and one-layer results. *Mon. Wea. Rev.,* **122,** 183–204.

——, and S. E. Cohn, 1994: Suboptimal schemes for atmospheric data assimilation based on the Kalman filter. *Mon. Wea. Rev.,* **122,** 2530–2557.

Verlaan, M., and A. W. Heemink, 1995: Reduced rank square root filters for large scale date assimilation problems. Proc., *Int. Symp. on Assimilation of Observations in Meteorology and Oceanography*, Tokyo, Japan, World Meteor. Org., 247–252.